Topology Reasoning for Driving Scenes

Tianyu Li^{1*}, Li Chen^{1,3*†}, Xiangwei Geng¹, Huijie Wang¹, Yang Li¹, Zhenbo Liu² Shengyin Jiang¹, Yuting Wang¹, Hang Xu², Chunjing Xu², Feng Wen², Ping Luo³ Junchi Yan⁴, Wei Zhang², Xiaogang Wang¹, Yu Qiao¹, Hongyang Li^{1,4†}

OpenDriveLab, Shanghai AI Laboratory
 Huawei Noah's Ark Lab
 The University of Hong Kong
 Shanghai Jiao Tong University
 *Equal contribution
 †Project lead

https://github.com/OpenDriveLab/TopoNet

Abstract

Understanding the road genome is essential to realize autonomous driving. This highly intelligent problem contains two aspects - the connection relationship of lanes, and the assignment relationship between lanes and traffic elements, where a comprehensive topology reasoning method is vacant. On one hand, previous map learning techniques struggle in deriving lane connectivity with segmentation or laneline paradigms; or prior lane topologyoriented approaches focus on centerline detection and neglect the interaction modeling. On the other hand, the traffic element to lane assignment problem is limited in the image domain, leaving how to construct the correspondence from two views an unexplored challenge. To address these issues, we present **TopoNet**, the first end-to-end framework capable of abstracting traffic knowledge beyond conventional perception tasks. To capture the driving scene topology, we introduce three key designs: (1) an embedding module to incorporate semantic knowledge from 2D elements into a unified feature space; (2) a curated scene graph neural network to model relationships and enable feature interaction inside the network; (3) instead of transmitting messages arbitrarily, a scene knowledge graph is devised to differentiate prior knowledge from various types of the road genome. We evaluate TopoNet on the challenging scene understanding benchmark, OpenLane-V2, where our approach outperforms all previous works by a great margin on all perceptual and topological metrics. The code would be released.

1. Introduction

Imagine that an autonomous vehicle is navigating towards a complex intersection and planning to go straight: it is wondering which one of the lanes in front to drive into and which traffic signal to follow. This high-level intellec-

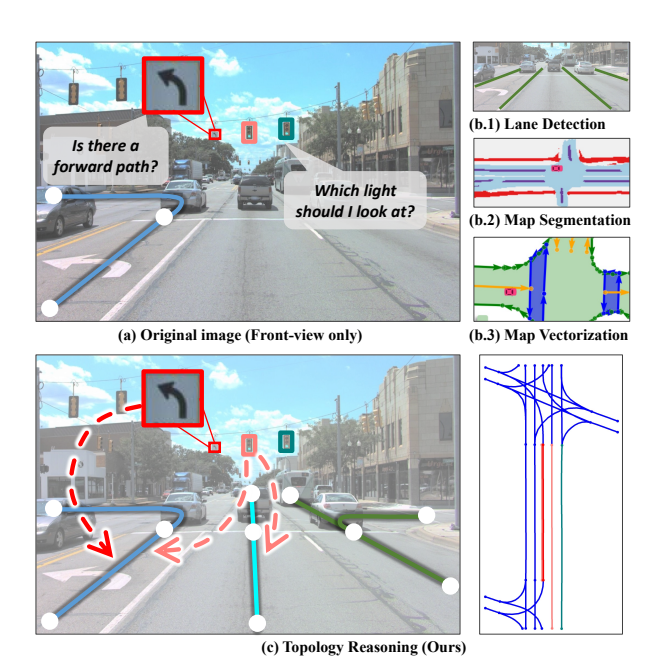


Figure 1. **Motivation of topology reasoning** for driving scenes. (a) While driving into an intersection, the self-driving vehicle has to reason about the correct lane and traffic information for downstream navigation. (b) Conventional map learning paradigms [53, 56, 41] focus on physical road elements, and thus cannot generate high-level navigation signals without sophisticated rules. (c) We advocate, and present TopoNet, to directly achieve the topology understanding of lanes and traffic elements.

tual problem requires the vehicle not only to accurately perceive lanes, but also to understand the topology relationship from sensor inputs. Specifically, the driving scene topology includes: (1) the **lane topology graph** comprises centerlines as well as their connectivity, (2) and the **assignment relationship** between lanes and traffic elements (*e.g.*, traffic lights, traffic boards and, road markers). As illustrated in Fig. 1, they altogether provide explicit navigation signals for downstream tasks such as motion prediction and planning [2, 9].

Conventional autonomous driving systems cope with the problem via off-board generated High-Definition (HD) maps, which include both physical lanelines and the driving scene topology [4, 66, 47]. However, pre-built HD maps severely suffer from scalability due to their high cost to construct and the strict requirement of localization systems. As shown in Fig. 1(b), various formulations are proposed to perceive the surrounding environments on-the-fly to serve as a supplement of HD maps, such as 2D and 3D laneline detection [53, 59, 11], bird's-eye-view (BEV) segmentation [52, 56, 35], and BEV map vecterization [41, 38]. Yet, the vectorization-based methods still struggle in deriving lane connectivity, though they are capable of modeling instance-wise lanelines in complex shapes. The "tabularasa" resolution, that directly averages two neighboring lanelines to get centerlines and then connects into a lane graph, takes complicated hand-crafted rules and heavy burdens on post-processing. The challenge is much severer in urban intersections to link centerlines in two directions with a virtual line (e.g., the blue turning curve in Fig. 1(a)).

An intuitive approach to predict centerlines directly is to supervise the original laneline perception frameworks with centerline labels. Attempts are carried out based on anchorbased 3D laneline detection [19, 20] and BEV segmentation algorithms [69], but fail to predict overlapping centerlines in crossings. Recent studies STSU and TPLR [5, 6] employ a Transformer-based decoder to predict centerline instances and an MLP to output their connectivity. In these works, centerline queries attend the whole image, which potentially raises the risk of overfitting to surrounding background characteristics such as buildings and vegetation. It also increases the difficulty of finding useful information without explicit relationship modeling inside the network, resulting in longer training time or pre-training requirement (200 epochs or Cityscape [12] pre-training for STSU).

On the other hand, the relationship assignment problem between traffic elements and lanes from sensor inputs remains unexplored outside of the image domain (perspective view, PV). Previous work [33] tried to associate the ground truth of lanelines and lights on 2D images. But joining features of 2D traffic elements and lanes in 3D or BEV space is a different story.

To address these issues, we present a Topology Reasoning Network (**TopoNet**), which predicts the driving scene topology in an end-to-end manner. As an attempt to reason about scene topology in a single network, TopoNet comprises two branches with a shared feature extractor, for traffic elements and centerlines respectively. Motivated by the Transformer-based detection algorithms [8, 73], we employ instance queries to extract useful local features via the deformable attention mechanism, which restricts the attention

region and accelerates convergence. Since the clues for locating a specific centerline instance could be encoded in its neighbors and corresponding traffic elements, a Scene Graph Neural Network (SGNN) is devised to transmit messages among instance-level embeddings. Furthermore, we propose a scene knowledge graph to capture prior topological knowledge from entities of different types. Specifically, a series of GNNs are developed based on categories of traffic elements and the centerline connectivity relationship (i.e., predecessor, ego, successor). Updated queries are ultimately decoded as the perception results and driving scene topology. With the proposed designs, we substantiate TopoNet on the large-scale topology reasoning benchmark, OpenLane-V2 [51]. TopoNet outperforms state-ofthe-art approaches by 15-84% for centerline perception, and achieves times of performance in terms of the challenging topology reasoning task. Ablations are conducted to verify the effectiveness of our framework.

To sum up, our key contributions are as follows.

- We advocate the philosophy of abstracting the driving scenes as lane topology, and discuss the problem of reasoning connections between centerlines and traffic elements from sensor inputs. We hope it could contribute as a supplement to online HD map learning.
- We present TopoNet, which unifies heterogeneous feature learning and enhances feature interactions via the graph neural network architecture and the knowledge graph design. To the best of our knowledge, it is the first work to achieve comprehensive driving scene understanding with onboard sensors.
- We demonstrate the superiority of TopoNet on the challenging topology reasoning benchmark. Particularly, it outperforms all previous state-of-the-art methods by a wide margin on both perceptual and topological metrics and shows great robustness in complex urban scenarios.

2. Related Work

Lane Graph Learning has received abundant attention due to its pivotal role in autonomous driving. Prior works investigate generating road graphs [25, 1] or spatially denser lane graphs [26, 75, 24, 3] from aerial images. However, roads in aerial images are often occluded by trees and buildings, leading to inaccurate results. Recently, there has been a growing focus on producing lane graphs directly from vehicle-mounted sensor data. STSU [5] proposes a DETR-like neural network to detect centerlines and then derive their connectivity by a successive MLP module. Based on STSU, Can *et al.* [6] introduce additional minimal cycle queries to ensure proper order of overlapping lines. CenterLineDet [69] regards centerlines as vertices and designs a graph-updating model trained by imitation learning. It is also worth noticing that Tesla proposes the "language

of lanes" to represent the lane graph as a sentence [61]. The attention-based model recursively predicts lane tokens and their connectivity. In this work, we focus on explicitly modeling the centerline connectivity inside the network to enhance feature learning and indulging traffic elements in constructing the full driving scene graph.

HD Map Perception. With the trending popularity of BEV perception [54, 36, 72, 28, 18], recent works focus on learning HD Maps with segmentation and vectorized methods. Map segmentation aims at predicting the semantic meaning of each BEV grid, such as lanelines, pedestrian crossings, and drivable areas. These works differentiate from each other mainly in the perspective view to BEV transform module, i.e., IPM-based [68, 7], depthbased [43, 27], or Transformer-based [36, 31]. Though dense segmentation provides pixel-level information, it cannot touch down the complex relationship of overlapping elements. Li et al. [35] handles the problem by grouping and vectorizing the segmented map with complicated postprocessings. VectorMapNet [41] proposes to directly represent each map element as a sequence of points, which uses coarse key points to decode laneline locations sequentially. MapTR [38] further explores a unified permutation-based modeling approach for the sequence of points to eliminate the modeling ambiguity and improve performance and efficiency. In fact, since vectorization also enriches the direction information for lanelines, vectorization-based methods could be easily adapted to centerline perception by alternating the supervision. Recently, InstaGraM [58] constructs map elements as a graph by predicting vertices first and then utilizing a GNN module to detect edges. Its GNN produces all vertex features simultaneously, leading to the lack of instance-level interaction. Contrary to the aforementioned approaches, we leverage instance-wise feature transmission with a graph neural network, to extract prominent prediction hints from other elements in the topology graph.

Driving Scene Understanding mainly indicates summarizing positional relationships of elements in outdoor environments beyond perception [74, 62, 50, 45]. Previous works focus on utilizing the relationships of 2D bounding boxes for motion prediction [34, 49, 50, 16] and risk assessment [71, 46]. In the industrial context, Mobileye presents an optimization-based method to automatically construct lane topology and traffic light-to-lane relationships based on their internal data [47]. In the academy, Langenberg et al. [33] address the traffic light to lane assignment (TL2LA) problem with a convolutional network by taking heterogeneous metadata as additional inputs. In contrast, TopoNet takes RGB images only and additionally reasons about the topology for lane entities besides TL2LA. We instantiate TopoNet on the large-scale driving scene understanding benchmark, which covers complicated urban scenarios.

Graph Neural Network and its variants, such as graph convolutional network (GCN) [32], GraphSAGE [22], and GAT [63], are widely adopted to aggregate features of vertices and extract information from graph data [57]. Witnessing the impressive achievements of GNN in various fields (e.g., recommendation system and video understanding) [21, 55, 10, 48], researchers in the autonomous driving community also attempt to utilize it to process unstructured data. Weng et al. [64, 65] introduce GNN to capture interactions among agent features for 3D multi-object tracking. LaneGCN [37] constructs a lane graph from HD map, while others [16, 30, 29] model the relationship of moving agents and lanelines as a graph to improve the trajectory forecasting performance. Inspired by prior works, we design a GNN for the driving scene understanding task to enhance feature interaction and introduce a class-specific knowledge graph to better incorporate semantic information.

3. TopoNet

3.1. Problem Formulation

Given images from multi-view cameras mounted on a vehicle, the goal of TopoNet lies in two perspectives - perceiving entities and reasoning their relationships. As an instance-level representation is preferable for topology reasoning, a directed centerline is described as an ordered list of points. We denote it as $v_l = [p_0,...,p_{n-1}]$, where $p = (x,y,z) \in \mathbb{R}^3$ describes a point's coordinate in 3D space, p_0 and p_{n-1} are the starting and ending point respectively. Traffic elements are represented as 2D bounding boxes in different classes on the front-view images. All existing lanes V_l and traffic elements V_t within a predefined range are required to be detected.

On the perceived entities, the topology relationships are built. The connectivity of directed lanes establishes a maplike network on which vehicles can drive and is denoted as the lane graph (V_l, E_{ll}) , where the edge set $E_{ll} \subseteq V_l \times V_l$ is asymmetric. An entry (i,j) in E_{ll} is positive if and only if the ending point of the lane v_i is connected to the starting point of v_j . The graph $(V_l \cup V_t, E_{lt})$ describes the correspondence between lanes and traffic elements. It can be seen as a bipartite graph that positive edges only exist between V_l and V_t . Both edge sets are required to be predicted in the task of topology reasoning.

3.2. Overview

Fig. 2 illustrates the overall architecture of the proposed **TopoNet**. Given multi-view images as input, the feature extractor generates multi-scale image features, including the front-view feature $F_{\rm PV}$, and then convert them into a BEV feature $F_{\rm BEV}$ through a view transform module. Two independent decoders with the same deformable attention architecture [73] consume $F_{\rm PV}$ and $F_{\rm BEV}$ to produce instance-level embeddings Q_t and Q_l separately. The proposed

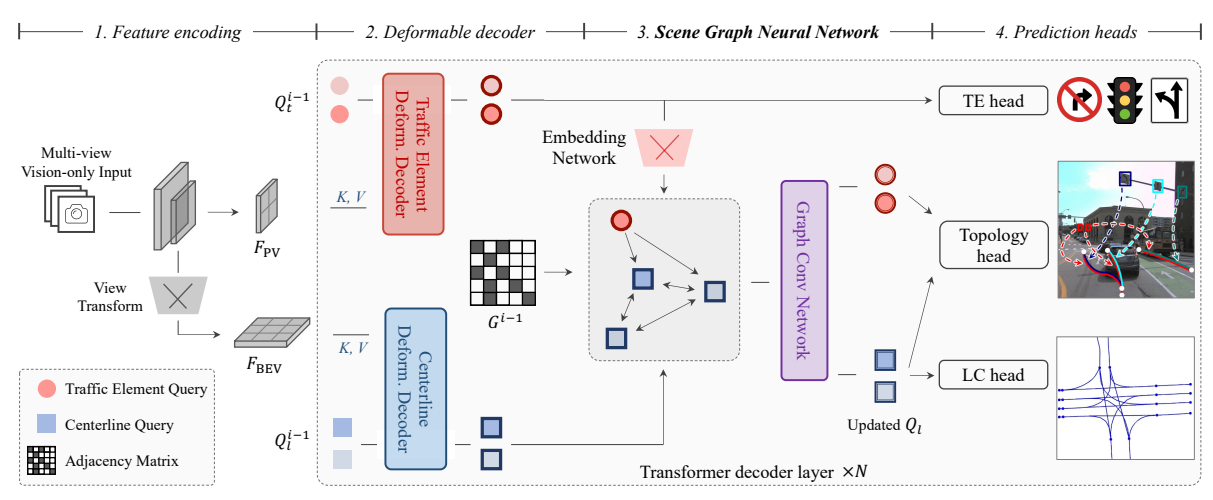


Figure 2. **Systematic diagram of TopoNet**. TopoNet addresses the crucial problem of topology reasoning for driving scenes in an end-to-end fashion. It consists of four stages, with the last three being compacted in a Transformer decoder architecture. TopoNet handles traffic elements and centerlines as two parallel branches at the Deformable decoder stage. Various types of instance queries (red, blue) then interact, exchange messages, acquire and aggregate prominent knowledge in the proposed Scene Graph Neural Network stage. The explicit relationship modeling inside the network serves as a favorable scheme for feature learning and topology prediction. We abbreviate traffic elements and lane centerlines as "TE" and "LC" in this paper, respectively.

Scene Graph Neural Network (SGNN) then refines centerline queries Q_l in positional and topological aspects. Note that the decoder and SGNN layers are stacked iteratively to obtain local and global features in a sequential fashion. Finally, the task-specific heads take the refined queries to produce prediction results. Next, we elaborate on the proposed SGNN module.

3.3. Scene Graph Neural Network

A representative embedding (or query) could provide ideal instance-wise detection or segmentation results, as discussed in conventional perception works [8, 67]. Nevertheless, being discriminative is not enough to recognize correct topology relationships. The reason is that it takes a pair of instance queries as input to determine their relationship, in which feature embeddings are actually not independent. Meanwhile, adopting the local feature aggregation scheme of point-wise queries [41, 38] for centerline perception is inadequate. Specifically, a key difference between centerlines and physical map elements is that centerlines naturally encode lane topology and traffic rules, which cannot be inferred from local features alone. Therefore, we aim to simultaneously acquire perception and reasoning results by modeling not only discriminative instance-level representations but also inter-entity relationships.

To this end, we present SGNN, which has several designs and merits compared to previous works. (1) It adopts an embedding network to extract TE knowledge within a unified feature space. (2) It models all entities in a frame as vertices in a graph, and strengthens interconnection among perceived instances to learn their inherent relationships with

a graph neural network. (3) Alongside the graph structure, SGNN incorporates prior topology knowledge with a scene knowledge graph. We detailedly introduce each part below.

Embedding Network. As traffic elements are labeled on the perspective view, it is hard to harness their positional features in the BEV space. However, their semantic meaning imposes a great effect that could not be neglected. For instance, a road sign indicating the prohibition of left turn usually corresponds to lanes that lay in the middle of the road. This predefined knowledge is beneficial for locating corresponding lanes. Towards this, we introduce an embedding network to extract semantic information and transform it into a unified feature space to match with centerlines:

$$\widetilde{Q}_t^i = \mathrm{embedding}^i \big(Q_t^i \big), \tag{1}$$

where i denotes the i-th decoder layer. Note that the queries \widetilde{Q}_t^i remain intact in the SGNN. This is intended since imagining traffic elements from centerlines is relatively challenging, and we empirically find that updating Q_t with too many feature interactions places negative effects on predicting their attributes.

Feature Propagation in GNN. In this part, we introduce how topological relationships are modeled and how knowledge from different queries is exchanged. Regarding the concept of relationship, GNN is a natural choice. Relations can be conveniently formulated as edges in a graph where entities are seen as vertices, while it is nontrivial in an open world without any explicit constraint. As there is no prior knowledge of topology structure, a trivial way is to construct a fully connected graph (V, E), where $V = V_l \cup V_t$

and $E \subseteq V \times V$. This inevitably increases computational cost and introduces unnecessary information transmission, such as between two traffic elements that are placed subjectively by humans. Instead, we form two directed graphs to propagate features, namely $G_{ll} = (V_l, V_l \times V_l)$ for lane graph estimation and $G_{lt} = (V_l \cup V_t, V_l \times V_t)$ representing the TE to LC assignments.

In graph G_{ll} and G_{lt} , lane queries Q_l are refined by the connected neighbors and corresponding traffic elements. Due to the fact that Q_l and Q_t represent different objects, the semantic gap still exists. We introduce an adapter layer to combine this heterogeneous information into the information gain denoted as R. The overall process in an SGNN layer can be formulated as follows:

$$\begin{split} Q_l^{i'} &= \operatorname{SGNN}_{ll}^i \big(Q_l^i, G_{ll}^{i-1}\big), \\ Q_l^{i''} &= \operatorname{SGNN}_{lt}^i \big(Q_l^i, \tilde{Q}_t^i, G_{lt}^{i-1}\big), \\ R^i &= \operatorname{downsample}^i \Big(\operatorname{ReLU} \big(\operatorname{concat}(Q_l^{i'}, Q_l^{i''}) \big) \Big), \\ \tilde{Q}_l^i &= Q_l^i + R^i. \end{split} \tag{2}$$

Next, we detail how the topological weights in SGNN are constructed and learned, based on a naive scene graph structure and an elaborately designed knowledge graph.

Vanilla Scene Graph. Given the adjacency matrix A_{ll}^{i-1} , which is a representation of G_{ll}^{i-1} from the previous layer, we construct a weight matrix T_{ll}^i to control the flow of messages in the graph. In the directed graph, messages are passed in a single direction, e.g., from a centerline to its successor. However, as the structure of lanes depends on each other, the position of a lane is a good indication of the locations of its neighbors. Thus, we supplement A_{ll}^{i-1} with a backward adjacency matrix to allow message exchange for two connected centerlines. The matrix T_{ll}^i of the i-th layer is calculated by:

$$\begin{split} T_{ll}^0 &= I, \\ T_{ll}^i &= \beta_{ll} \cdot \left(A_{ll}^{i-1} + \text{transpose}(A_{ll}^{i-1}) \right) + I, \end{split} \tag{3}$$

where I denotes the identical mapping for self-loop, β_{ll} is a hyperparameter to control the ratio of features propagated between nodes.

In the bipartite graph G_{lt} , where only the correspondence between lanes and traffic elements is presented, we utilize features of traffic elements to refine centerline embeddings as follows:

$$T_{lt}^{0} = O,$$

 $T_{lt}^{i} = \beta_{lt} \cdot A_{lt}^{i-1},$ (4)

where O is a matrix in which all entries are zero.

After obtaining the weight matrices, SGNN utilizes the graph convolutional layer (GCN) [32] to perform feature

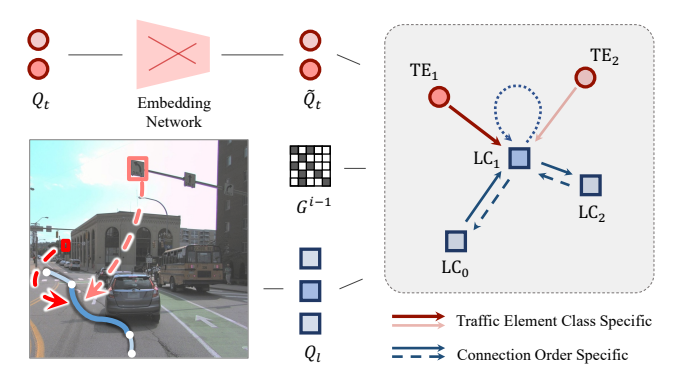


Figure 3. **Scene knowledge graph** illustration. For the centerline colored **blue** in the left case, related weight matrices in the graph are categorically independent. Different traffic elements and lane-directed connections bring different information to the centerline, which is encoded as a scene knowledge graph on the right.

propagation among queries:

$$Q_l^{i'} = \operatorname{GCN}_{ll}^i(Q_l^i, T_{ll}^i),$$

$$Q_l^{i''} = \operatorname{GCN}_{lt}^i(Q_l^i, \widetilde{Q}_t^i, T_{lt}^i).$$
(5)

Scene Knowledge Graph. Though GCN enables feature propagation in the built graphs and treats nodes differently based on their connectivity, the semantic meaning of vertices remains unexplored. For example, the information from a traffic element indicating to go straight is not equally important to a red light. To address the issue and incorporate categorical prior, we design the scene knowledge graph to treat vertices in different classes differently. Fig. 3 illustrates an example process of updating a centerline query LC_1 on the given knowledge graph.

On the graph G_{lt} , we use $\mathbf{W}_{lt}^i \in \mathbb{R}^{|C_t| \times F_l \times F_t}$ to denote the learnable weights, where C_t describes the attribute set of traffic elements, F_l and F_t are the number of feature channel of LC and TE queries respectively. A centerline query with index x aggregates information from its corresponding traffic elements based on their classification scores:

$$K_{lt}^{i} = A_{lt}^{i-1},$$

$$Q_{l_{(x)}}^{i''} = \sum_{\forall y \in N(x)} \sum_{\forall c_{t} \in C_{t}} \beta_{lt} \cdot S_{t_{(c_{t},y)}}^{i} K_{lt_{(x,y)}}^{i} \mathbf{W}_{lt_{(c_{t})}}^{i} \widetilde{Q}_{t_{(y)}}^{i},$$
(6)

where N(x) outputs the indices of all neighbors of the vertex with index x, and $S_t^i \in \mathbb{R}^{|C_t| \times |Q_t^i|}$ represents the classification scores of traffic element queries.

Although all centerlines fall into the same category, the directed connection nature, namely predecessor and successor, still poses an impact on the process of feature propagation. To this end, we formulate the learnable weight matrix for the lane graph as $\mathbf{W}_{ll}^i \in \mathbb{R}^{|C_l| \times F_l \times F_l}$, where $C_l = \{\text{successor}, \text{predecessor}, \text{self-loop}\}$. The centerline

queries are further updated by:

$$\begin{split} K^i_{ll} &= \operatorname{stack} \left(A^{i-1}_{ll}, \operatorname{transpose}(A^{i-1}_{ll}), I\right), \\ Q^{i'}_{l(x)} &= \sum_{\forall y \in N(x)} \sum_{\forall c_l \in C_l} \beta_{ll} \cdot K^i_{ll(c_l, x, y)} \mathbf{W}^i_{ll(c_l)} Q^i_{l(y)}. \end{split} \tag{7}$$

3.4. Learning

We employ multiple losses to train TopoNet in an end-to-end manner. As depicted in Fig. 2, all heads consume queries to provide perception and reasoning results. Nevertheless, they are not entirely independent, as the topology head requires matching results from perception heads. Similar to Transfomer-based networks [8, 73], the supervision is applied on each decoder layer to optimize the query feature iteratively. The overall loss of the proposed model is:

$$\mathcal{L} = \mathcal{L}_{det_{\text{TE}}} + \mathcal{L}_{det_{\text{LC}}} + \mathcal{L}_{top}.$$
 (8)

Perception. Following the head design in DETR [8], the TE head predicts 2D bounding boxes with classification scores. Note that for predicting traffic elements, we take Q_t instead of Q_t to preserve their positional information in the perspective view. The LC head produces 11 ordered 3D points and a confidence score from each centerline query $\tilde{q}_l \in Q_l$. The ground truth of centerlines is normalized based on the predefined BEV range. For both heads, the Hungarian algorithm is utilized to generate matchings between ground truth and predictions, with the matching cost the same as the loss function. Then task-specific losses $\mathcal{L}_{det_{ ext{TE}}}$ and $\mathcal{L}_{det_{ ext{LC}}}$ are applied accordingly. Specifically, for the TE head, we employ the Focal loss [40] for classification, an L1 regression loss, and an IOU loss for localization. Meanwhile, for centerlines, we use Focal loss and L1 loss as the classification and regression loss, respectively.

Reasoning. The topology head reasons pairwise relationships on the given embeddings. Similar to STSU [5], for a pair of instances, we use two MLP layers to reduce the feature dimension for each instance. Then the concatenated feature is sent into another MLP with a sigmoid activation to predict their relationship. Based on the matching results from perception heads, the ground truth of each pair of embeddings is assigned. Different from the TE head, we adopt embeddings from the SGNN module, *i.e.*, the refined queries \widetilde{Q}_l for lanes and the semantic embeddings \widetilde{Q}_t for traffic elements. Due to the sparsity of the graph, there exists a severe imbalance in sample distribution, towards which the Focal loss is deployed in \mathcal{L}_{top} .

4. Experiments

4.1. Protocols

Dataset and Metrics. We conduct experiments on the challenging OpenLane-V2 benchmark [51], which covers

complex urban scenarios. It comprises 960K instancelevel annotations and 891K topology relationship labels. The dataset contains 1,000 scenes of roughly 15s duration with multi-view images from 7 cameras and annotations at 2Hz. All lanes within [-50m, +50m] along the x-axis and [-25m, +25m] along the y-axis are annotated in the 3D space, while traffic elements are labeled as 2D bounding boxes on the front-view images. The topology relationships are provided in the form of adjacency matrices based on the ordering of centerlines and traffic elements. We adopt the official evaluation metrics of the benchmark. DET_l and DET_t measure instance-level perception performance on centerlines and traffic elements. Note that DET₁ represents the mean average precision averaged over multiple Fréchet distances [14] thresholded on {1.0, 2.0, 3.0}. To better align with previous works [41, 38], we also provide $\mathrm{DET}_{l,\mathrm{chamfer}}$ with the Chamfer distance as the similarity measure. It does not take the lane direction into account and is thresholded on $\{0.5, 1.0, 1.5\}$. For topology reasoning, TOP_{ll} and TOP_{lt} are utilized to evaluate relationship prediction among centerlines and between centerlines and traffic elements respectively. More details are provided in the appendix.

Implementation Details. We adopt ResNet-50 [23] pretrained on ImageNet [13] as the image backbone. A deformable DETR encoder [73] is employed to encode the PV feature, while a BEVFormer encoder [36] without temporal information is adapted to construct the BEV feature. We adopt the AdamW optimizer [44] and a cosine annealing schedule with an initial learning rate of 1×10^{-4} . TopoNet is trained for 24 epochs with a batch size of 8 with 8 NVIDIA Tesla A100 GPUs. β_{ll} and β_{lt} are set to 0.5 in our experiments. We put correlated details in the appendix.

Baselines. Since there are no prior methods for the task of driving scene understanding, we adapt three state-of-the-art algorithms which are initially designed for lane graph estimation or map learning: STSU [5], VectorMapNet [41], and MapTR [38]. For a fair comparison, we utilize the same image backbone and adopt the same TE head as in TopoNet.

As for topology reasoning, we treat it differently based on their own modeling concepts. Specifically, STSU predicts centerlines as Bezier curves and their relationships. Thus most of its designs are retained, while other irrelevant modules are removed. Additionally, we append a topology head for predicting correspondence between centerlines and traffic elements. The goal of VectorMapNet and MapTR is to predict vectorized map elements such as lanelines and pedestrian crossings. VectorMapNet utilizes a DETR-like decoder to estimate key points and then introduces an autoregressive module to generate detailed graphical information for a laneline instance. MapTR directly predicts polylines with a fixed number of points using a Transformer

decoder. To adapt them to our task, we supervise VectorMapNet and MapTR with centerline labels and use the element queries in their Transformer decoders as the instance queries to produce the driving scene topology.

4.2. Main Results

We compare the proposed TopoNet to several state-ofthe-art methods in Table 1. On the validation set, TopoNet outperforms all previous algorithms by a large margin in both directed centerline perception and lane topology reasoning (DET_l +10.1%, TOP_{ll} +2.4%, and TOP_{lt} +4.8%). The SOTA map learning method MapTR ignores the direction of centerlines with the permutation-equivalent modeling, and achieves competitive performance under $DET_{l,chamfer}$. However, its performance on DET_l as well as topology metrics significantly degenerates. We additionally evaluate MapTR based on Chamfer distance matching. In this circumstance, MapTR achieves an acceptable performance on lane-TE relationship prediction, but still struggles in lane graph estimation. The performance of centerline queries without directional information indicates that understanding the complex scenario and perceiving presented instances are two totally different stories.

To evaluate the robustness of various approaches, we further divide the validation data into two splits, *i.e.*, crossings and geographical isolation. We can observe that though TopoNet has a performance degradation, it still showcases superior performance over previous methods.

We provide a qualitative comparison in Fig. 4. TopoNet predicts most centerlines correctly and constructs a lane graph in BEV. Yet, prior works fail to output all entities or get confused about their connectivity. More visualizations as well as the analysis of failure cases are in the appendix.

4.3. Ablation Study

Scene Graph Neural Network. For ablations on the proposed SGNN, we alternate the proposed network into a baseline without feature propagation by setting β_{ll} and β_{lt} to 0, in which the SGNN module is downgraded to an MLP. As illustrated in Table 2, the proposed SKG outperforms models in other settings, demonstrating its effectiveness for topology understanding.

By comparing "LL only" models, which means only the graph G_{ll} is applied, to the baseline, we can observe that the SKG design shows consistent improvement in centerline perception (DET_l +0.6%) and topology reasoning (TOP_{lt} +0.9%), with the help of semantic information. However, by directly mixing predecessor and successor information in the SG version, detrimental performance is observed, indicating that information obtained from predecessors and successors is not equally important.

With the "LT only" design, TopoNet gains significantly in topology reasoning on both the SG and the SKG structure (TOP $_{ll}$ +1.6% and +1.2% respectively). Furthermore, the

Data	Method	$DET_l\uparrow$	$\mathrm{DET}_{l,\mathrm{chamfer}} \uparrow$	$TOP_{ll}\uparrow$	$\mathrm{TOP}_{lt} \uparrow$
	STSU [5]	12.0	11.5	0.3	10.1
	VectorMapNet [41]	11.3	13.4	0.1	6.2
ΑΠ	MapTR [38]	8.3	<u>17.7</u>	0.2	5.8
•	MapTR* [38]	8.3	<u>17.7</u>	<u>1.1</u>	10.1
	TopoNet (Ours)	22.1	20.2	2.7	14.9
	STSU [5]	10.8	7.4	0.1	8.3
Crossings	VectorMapNet [41]	<u>11.8</u>	11.4	0.0	5.5
ssi	MapTR [38]	7.0	<u>15.9</u>	0.1	4.5
2	MapTR* [38]	7.0	<u>15.9</u>	0.8	8.2
	TopoNet (Ours)	19.7	18.2	2.1	10.8
_ uo	STSU [5]	9.2	10.0	0.4	7.1
lati	VectorMapNet [41]	8.1	6.3	0.1	5.1
Geo. Isolation	MapTR [38]	7.6	12.9	0.2	4.8
· · ·	MapTR* [38]	7.6	12.9	0.8	<u>8.1</u>
g	TopoNet (Ours)	14.2	<u>12.6</u>	1.2	10.4

Table 1. Comparison with state-of-the-art methods under three data splits. TopoNet outperforms all previous works by a wide margin, especially in directed centerline perception and topology reasoning. It also demonstrates the robustness in complex scenarios and brand-new geographical regions. "Crossings" refers to frames where over 30% of centerlines are inside intersections. "Geo. Isolation" denotes the partial validation frames under completely distinct locations from the training set. *: Topology reasoning evaluation is based on matching results on Chamfer distance. The highest score is bolded, while the second one is underlined.

scene knowledge graph provides an additional improvement of 1.0% for centerline perception, owning to the predefined semantic prior encoded in the categories of traffic elements.

When taking both graphs into consideration, SKG outperforms the baseline model by 1.1% on centerline detection and 1.3% on topology reasoning between centerlines and traffic elements. The improvement of traffic element detection and lane topology prediction is also consistent. We can also summarize that the SG version benefits from the combination of spatial information from neighboring lanes and corresponding traffic elements, and it even slightly outperforms the SKG version in lane-traffic element relationship prediction. Similar trends are observed in the "LT only" designs as well, suggesting that SKG's modeling of relationships has a negative impact on the representation learning of TE embeddings. It further leads to performance degradation in lane-traffic element relationship prediction, which is worth to be explored in future work.

Traffic Element Embedding. We provide ablations on the proposed embedding network for traffic elements in Table 3. Removing the embedding results in a 3.0% performance drop in centerline detection and a 0.1% drop in lane graph prediction. TE queries without embedding contain a large amount of spatial information in the PV space due to the 2D detection supervision signals. It results in significant inconsistencies in the feature spaces, which can also be verified from the performance of traffic element detection: the model without the embedding network slightly outperforms



Figure 4. **Qualitative results** of TopoNet and other algorithms. While driving into a complex urban crossing, TopoNet achieves superior lane graph prediction performance compared to other SOTA methods (bottom row). It also successfully builds all connections between traffic elements and lanes (top right, and correspondingly colored lines in BEV). Colors denote categories of traffic elements.

Type	Method	$\mathrm{DET}_l \uparrow$	$TOP_{ll} \!\!\uparrow$	$\mathrm{DET}_t \!\!\uparrow$	$\mathrm{TOP}_{lt} \!\!\uparrow$
-	Baseline	21.0	2.4	58.0	13.6
SG	+ LL only + LT only TopoNet-SG	20.9 21.0 21.7	2.4 2.6 2.4	60.8 60.3 61.6	13.0 15.2 15.5
SKG	+ LL only + LT only TopoNet-SKG	21.6 22.0 22.1	2.5 2.7 2.7	59.2 59.4 59.1	14.5 14.8 14.9

Table 2. Ablation on the design of scene graph neural network. The perception and topology reasoning tasks benefit from modeling centerline connections, traffic elements to lane assignments, and prior knowledge via SGNN. "SG" represents the vanilla scene graph, and "SKG" is the enhanced SGNN with the proposed scene knowledge graph. "LL only" denotes that SGNN only aggregates the spatial information from lane-lane connectivity, and "LT only" indicates that only semantic information from the lane-traffic element relationship is included in SGNN.

TopoNet in this case. In all, the experiments demonstrate that TE embedding effectively filters out irrelevant spatial information and extracts high-level semantic knowledge to help centerline detection and lane topology reasoning.

5. Conclusion and Future Work

In this paper, we discuss abstracting driving scenes as topology relationships and propose the first resolution,

Method	$DET_l\uparrow$	$\mathrm{DET}_{l,\mathrm{chamfer}} \uparrow$	$TOP_{ll}\uparrow$	$\mathrm{DET}_t \uparrow$	$TOP_{lt} \!\!\uparrow$
w/o embedding	19.1	18.2	2.6	59.8	14.9
TopoNet	22.1	20.2	2.7	59.1	14.9

Table 3. **Ablation on traffic element embedding.** TE embedding effectively filters out irrelevant spatial information in the PV space and extracts high-level semantic knowledge to help centerline detection and lane topology reasoning.

namely TopoNet, to address the problem. Importantly, our method models feature interactions via the graph neural network architecture and incorporate traffic knowledge in heterogeneous feature spaces with the knowledge graph-based design. Our experiments on the large-scale OpenLane-V2 benchmark demonstrate that TopoNet excels prior SOTA approaches on perceiving and reasoning about the driving scene topology under complex urban scenarios.

Limitations and Future Work. Due to the query-based design for feature interactions, TopoNet performs well in achieving most positive predictions, while post-processes such as merging or pruning are still needed to produce clean output as in lane topology works [5, 3]. How to incorporate the merging ability with auto-regressive or other association mechanisms deserves future exploration. Meanwhile, it will be interesting to see if more categories of traffic elements, and correspondingly more sophisticated knowledge graphs will make any advances if a suitable dataset is available.

References

- [1] Wele Gedara Chaminda Bandara, Jeya Maria Jose Valanarasu, and Vishal M Patel. Spin road mapper: Extracting roads from aerial images via spatial and interaction space graph reasoning for autonomous driving. In *ICRA*, 2022. 2
- [2] Mayank Bansal, Alex Krizhevsky, and Abhijit Ogale. Chauffeurnet: Learning to drive by imitating the best and synthesizing the worst. arXiv preprint arXiv:1812.03079, 2018. 2
- [3] Martin Büchner, Jannik Zürn, Ion-George Todoran, Abhinav Valada, and Wolfram Burgard. Learning and aggregating lane graphs for urban automated driving. *arXiv preprint arXiv:2302.06175*, 2023. 2, 8
- [4] Holger Caesar, Varun Bankiti, Alex H Lang, Sourabh Vora, Venice Erin Liong, Qiang Xu, Anush Krishnan, Yu Pan, Giancarlo Baldan, and Oscar Beijbom. nuscenes: A multimodal dataset for autonomous driving. In CVPR, 2020. 2
- [5] Yigit Baran Can, Alexander Liniger, Danda Pani Paudel, and Luc Van Gool. Structured bird's-eye-view traffic scene understanding from onboard images. In *ICCV*, 2021. 2, 6, 7, 8, 14, 15
- [6] Yigit Baran Can, Alexander Liniger, Danda Pani Paudel, and Luc Van Gool. Topology preserving local road network estimation from single onboard camera image. In CVPR, 2022.
- [7] Yigit Baran Can, Alexander Liniger, Ozan Unal, Danda Paudel, and Luc Van Gool. Understanding bird's-eye view of road semantics using an onboard camera. *IEEE RA-L*, 2022. 3
- [8] Nicolas Carion, Francisco Massa, Gabriel Synnaeve, Nicolas Usunier, Alexander Kirillov, and Sergey Zagoruyko. End-toend object detection with transformers. In ECCV, 2020. 2, 4, 6
- [9] Yuning Chai, Benjamin Sapp, Mayank Bansal, and Dragomir Anguelov. Multipath: Multiple probabilistic anchor trajectory hypotheses for behavior prediction. In CoRL, 2020. 2
- [10] Xiaojun Chang, Pengzhen Ren, Pengfei Xu, Zhihui Li, Xiaojiang Chen, and Alex Hauptmann. A comprehensive survey of scene graphs: Generation and application. *IEEE TPAMI*, 2021. 3
- [11] Li Chen, Chonghao Sima, Yang Li, Zehan Zheng, Jiajie Xu, Xiangwei Geng, Hongyang Li, Conghui He, Jianping Shi, Yu Qiao, and Junchi Yan. PersFormer: 3d lane detection via perspective transformer and the openlane benchmark. In ECCV, 2022. 2
- [12] Marius Cordts, Mohamed Omran, Sebastian Ramos, Timo Rehfeld, Markus Enzweiler, Rodrigo Benenson, Uwe Franke, Stefan Roth, and Bernt Schiele. The cityscapes dataset for semantic urban scene understanding. In CVPR, 2016. 2
- [13] Jia Deng, Wei Dong, Richard Socher, Li-Jia Li, Kai Li, and Li Fei-Fei. Imagenet: A large-scale hierarchical image database. In CVPR, 2009. 6
- [14] Thomas Eiter and Heikki Mannila. Computing discrete fréchet distance. 1994. 6, 13
- [15] Haoqiang Fan, Hao Su, and Leonidas J Guibas. A point set generation network for 3d object reconstruction from a single image. In CVPR, 2017. 13

- [16] Jianwu Fang, Chen Zhu, Pu Zhang, Hongkai Yu, and Jianru Xue. Heterogeneous trajectory forecasting via risk and scene graph learning. arXiv preprint arXiv:2211.00848, 2022. 3
- [17] Jiyang Gao, Chen Sun, Hang Zhao, Yi Shen, Dragomir Anguelov, Congcong Li, and Cordelia Schmid. Vectornet: Encoding hd maps and agent dynamics from vectorized representation. In CVPR, 2020. 14
- [18] Yulu Gao, Chonghao Sima, Shaoshuai Shi, Shangzhe Di, Si Liu, and Hongyang Li. Sparse dense fusion for 3d object detection. *arXiv preprint arXiv:2304.04179*, 2023. 3
- [19] Noa Garnett, Rafi Cohen, Tomer Pe'er, Roee Lahav, and Dan Levi. 3d-lanenet: End-to-end 3d multiple lane detection. In *ICCV*, 2019. 2
- [20] Yuliang Guo, Guang Chen, Peitao Zhao, Weide Zhang, Jinghao Miao, Jingao Wang, and Tae Eun Choe. Gen-lanenet: A generalized and scalable approach for 3d lane detection. In ECCV, 2020. 2
- [21] Zhiwei Guo and Heng Wang. A deep graph neural network-based mechanism for social recommendations. *IEEE TII*, 2020. 3
- [22] Will Hamilton, Zhitao Ying, and Jure Leskovec. Inductive representation learning on large graphs. In *NeurIPS*, 2017. 3
- [23] Kaiming He, Xiangyu Zhang, Shaoqing Ren, and Jian Sun. Deep residual learning for image recognition. In CVPR, 2016. 6, 12
- [24] Songtao He and Hari Balakrishnan. Lane-level street map extraction from aerial imagery. In WACV, 2022. 2
- [25] Songtao He, Favyen Bastani, Satvat Jagwani, Mohammad Alizadeh, Hari Balakrishnan, Sanjay Chawla, Mohamed M Elshrif, Samuel Madden, and Mohammad Amin Sadeghi. Sat2graph: Road graph extraction through graph-tensor encoding. In ECCV, 2020. 2
- [26] Namdar Homayounfar, Wei-Chiu Ma, Justin Liang, Xinyu Wu, Jack Fan, and Raquel Urtasun. Dagmapper: Learning to map by discovering lane topology. In *ICCV*, 2019. 2
- [27] Shengchao Hu, Li Chen, Penghao Wu, Hongyang Li, Junchi Yan, and Dacheng Tao. ST-P3: End-to-end vision-based autonomous driving via spatial-temporal feature learning. In ECCV, 2022. 3
- [28] Yihan Hu, Jiazhi Yang, Li Chen, Keyu Li, Chonghao Sima, Xizhou Zhu, Siqi Chai, Senyao Du, Tianwei Lin, Wenhai Wang, Lewei Lu, Xiaosong Jia, Qiang Liu, Jifeng Dai, Yu Qiao, and Hongyang Li. Planning-oriented autonomous driving. In CVPR, 2023. 3
- [29] Xiaosong Jia, Li Chen, Penghao Wu, Jia Zeng, Junchi Yan, Hongyang Li, and Yu Qiao. Towards capturing the temporal dynamics for trajectory prediction: a coarse-to-fine approach. In CoRL, 2022. 3
- [30] Xiaosong Jia, Penghao Wu, Li Chen, Hongyang Li, Yu Liu, and Junchi Yan. HDGT: Heterogeneous driving graph transformer for multi-agent trajectory prediction via scene encoding. arXiv preprint arXiv:2205.09753, 2022. 3
- [31] Yanqin Jiang, Li Zhang, Zhenwei Miao, Xiatian Zhu, Jin Gao, Weiming Hu, and Yu-Gang Jiang. Polarformer: Multicamera 3d object detection with polar transformers. In AAAI, 2023. 3

- [32] Thomas N Kipf and Max Welling. Semi-supervised classification with graph convolutional networks. In *ICLR*, 2017. 3, 5, 12
- [33] Tristan Langenberg, Timo Lüddecke, and Florentin Wörgötter. Deep metadata fusion for traffic light to lane assignment. *IEEE RA-L*, 2019. 2, 3
- [34] Chengxi Li, Yue Meng, Stanley H Chan, and Yi-Ting Chen. Learning 3d-aware egocentric spatial-temporal interaction via graph convolutional networks. In *ICRA*, 2020. 3
- [35] Qi Li, Yue Wang, Yilun Wang, and Hang Zhao. Hdmapnet: An online hd map construction and evaluation framework. In *ICRA*, 2022. 2, 3, 15, 16
- [36] Zhiqi Li, Wenhai Wang, Hongyang Li, Enze Xie, Chonghao Sima, Tong Lu, Qiao Yu, and Jifeng Dai. BEVFormer: Learning bird's-eye-view representation from multi-camera images via spatiotemporal transformers. In *ECCV*, 2022. 3, 6, 12, 16
- [37] Ming Liang, Bin Yang, Rui Hu, Yun Chen, Renjie Liao, Song Feng, and Raquel Urtasun. Learning lane graph representations for motion forecasting. In ECCV, 2020. 3
- [38] Bencheng Liao, Shaoyu Chen, Xinggang Wang, Tianheng Cheng, Qian Zhang, Wenyu Liu, and Chang Huang. MapTR: Structured modeling and learning for online vectorized HD map construction. In *ICLR*, 2023. 2, 3, 4, 6, 7, 14, 15
- [39] Tsung-Yi Lin, Piotr Dollár, Ross Girshick, Kaiming He, Bharath Hariharan, and Serge Belongie. Feature pyramid networks for object detection. In *CVPR*, 2017. 12
- [40] Tsung-Yi Lin, Priya Goyal, Ross Girshick, Kaiming He, and Piotr Dollár. Focal loss for dense object detection. In *ICCV*, 2017. 6
- [41] Yicheng Liu, Yue Wang, Yilun Wang, and Hang Zhao. Vectormapnet: End-to-end vectorized hd map learning. *arXiv* preprint arXiv:2206.08920, 2022. 1, 2, 3, 4, 6, 7, 15, 16
- [42] Ze Liu, Yutong Lin, Yue Cao, Han Hu, Yixuan Wei, Zheng Zhang, Stephen Lin, and Baining Guo. Swin transformer: Hierarchical vision transformer using shifted windows. In *ICCV*, 2021. 16
- [43] Zhijian Liu, Haotian Tang, Alexander Amini, Xingyu Yang, Huizi Mao, Daniela Rus, and Song Han. BEVFusion: Multitask multi-sensor fusion with unified bird's-eye view representation. In *ICRA*, 2023. 3, 16
- [44] Ilya Loshchilov and Frank Hutter. Decoupled weight decay regularization. In *ICLR*, 2018. 6
- [45] Arnav Vaibhav Malawade, Shih-Yuan Yu, Brandon Hsu, Harsimrat Kaeley, Anurag Karra, and Mohammad Abdullah Al Faruque. Roadscene2vec: A tool for extracting and embedding road scene-graphs. *Knowledge-Based Systems*, 2022. 3
- [46] Arnav Vaibhav Malawade, Shih-Yuan Yu, Brandon Hsu, Deepan Muthirayan, Pramod P Khargonekar, and Mohammad Abdullah Al Faruque. Spatiotemporal scene-graph embedding for autonomous vehicle collision prediction. *IoT-J*, 2022. 3
- [47] Mobileye. Mobileye under the hood. https://www.mobileye.com/ces-2022/, 2022. 2, 3
- [48] Abduallah Mohamed, Kun Qian, Mohamed Elhoseiny, and Christian Claudel. Social-stgcnn: A social spatio-temporal

- graph convolutional neural network for human trajectory prediction. In CVPR, 2020. 3
- [49] Sravan Mylavarapu, Mahtab Sandhu, Priyesh Vijayan, K Madhava Krishna, Balaraman Ravindran, and Anoop Namboodiri. Towards accurate vehicle behaviour classification with multi-relational graph convolutional networks. In IV, 2020. 3
- [50] Sravan Mylavarapu, Mahtab Sandhu, Priyesh Vijayan, K Madhava Krishna, Balaraman Ravindran, and Anoop Namboodiri. Understanding dynamic scenes using graph convolution networks. In *IROS*, 2020. 3
- [51] OpenLane-V2 Dataset Contributors. OpenLane-V2: The World's First Perception and Reasoning Benchmark for Scene Structure in Autonomous Driving, 2023. 2, 6, 13, 16
- [52] Bowen Pan, Jiankai Sun, Ho Yin Tiga Leung, Alex Andonian, and Bolei Zhou. Cross-view semantic segmentation for sensing surroundings. *IEEE RA-L*, 2020. 2
- [53] Xingang Pan, Jianping Shi, Ping Luo, Xiaogang Wang, and Xiaoou Tang. Spatial as deep: Spatial cnn for traffic scene understanding. In AAAI, 2018. 1, 2
- [54] Jonah Philion and Sanja Fidler. Lift, splat, shoot: Encoding images from arbitrary camera rigs by implicitly unprojecting to 3d. In ECCV, 2020. 3
- [55] P Pradhyumna and GP Shreya. Graph neural network (gnn) in image and video understanding using deep learning for computer vision applications. In *ICESC*, 2021. 3
- [56] Thomas Roddick and Roberto Cipolla. Predicting semantic map representations from images using pyramid occupancy networks. In CVPR, 2020. 1, 2
- [57] Franco Scarselli, Marco Gori, Ah Chung Tsoi, Markus Hagenbuchner, and Gabriele Monfardini. The graph neural network model. *IEEE TNNLS*, 2008. 3
- [58] Juyeb Shin, Francois Rameau, Hyeonjun Jeong, and Dongsuk Kum. Instagram: Instance-level graph modeling for vectorized hd map learning. arXiv preprint arXiv:2301.04470, 2023. 3
- [59] Lucas Tabelini, Rodrigo Berriel, Thiago M Paixao, Claudine Badue, Alberto F De Souza, and Thiago Oliveira-Santos. Keep your eyes on the lane: Real-time attention-guided lane detection. In CVPR, 2021. 2
- [60] Mingxing Tan and Quoc Le. Efficientnet: Rethinking model scaling for convolutional neural networks. In *ICML*, 2019.
 14
- [61] Tesla. Tesla AI Day. https://www.youtube.com/ watch?v=ODSJsviD_SU, 2022. 3
- [62] Yafu Tian, Alexander Carballo, Ruifeng Li, and Kazuya Takeda. Road scene graph: A semantic graph-based scene representation dataset for intelligent vehicles. arXiv preprint arXiv:2011.13588, 2020. 3
- [63] Petar Veličković, Guillem Cucurull, Arantxa Casanova, Adriana Romero, Pietro Lio, and Yoshua Bengio. Graph attention networks. In *ICLR*, 2018. 3
- [64] Xinshuo Weng, Yongxin Wang, Yunze Man, and Kris M Kitani. Gnn3dmot: Graph neural network for 3d multi-object tracking with 2d-3d multi-feature learning. In CVPR, 2020.

- [65] Xinshuo Weng, Ye Yuan, and Kris Kitani. Ptp: Parallelized tracking and prediction with graph neural networks and diversity sampling. *IEEE RA-L*, 2021. 3
- [66] Benjamin Wilson, William Qi, Tanmay Agarwal, John Lambert, Jagjeet Singh, Siddhesh Khandelwal, Bowen Pan, Ratnesh Kumar, Andrew Hartnett, Jhony Kaesemodel Pontes, Deva Ramanan, Peter Carr, and James Hays. Argoverse 2: Next generation datasets for self-driving perception and forecasting. In *NeurIPS*, 2021. 2, 16
- [67] Junfeng Wu, Yi Jiang, Song Bai, Wenqing Zhang, and Xiang Bai. Seqformer: Sequential transformer for video instance segmentation. In ECCV, 2022. 4
- [68] Enze Xie, Zhiding Yu, Daquan Zhou, Jonah Philion, Anima Anandkumar, Sanja Fidler, Ping Luo, and Jose M Alvarez. M²BEV: Multi-camera joint 3d detection and segmentation with unified birds-eye view representation. arXiv preprint arXiv:2204.05088, 2022. 3
- [69] Zhenhua Xu, Yuxuan Liu, Yuxiang Sun, Ming Liu, and Lujia Wang. Centerlinedet: Road lane centerline graph detection with vehicle-mounted sensors by transformer for highdefinition map creation. In *ICRA*, 2023. 2
- [70] Chenyu Yang, Yuntao Chen, Hao Tian, Chenxin Tao, Xizhou Zhu, Zhaoxiang Zhang, Gao Huang, Hongyang Li, Yu Qiao, Lewei Lu, et al. BEVFormer v2: Adapting modern image backbones to bird's-eye-view recognition via perspective supervision. In CVPR, 2023. 12
- [71] Shih-Yuan Yu, Arnav Vaibhav Malawade, Deepan Muthirayan, Pramod P Khargonekar, and Mohammad Abdullah Al Faruque. Scene-graph augmented data-driven risk assessment of autonomous vehicle decisions. *IEEE T-ITS*, 2021.
- [72] Brady Zhou and Philipp Krähenbühl. Cross-view transformers for real-time map-view semantic segmentation. In CVPR, 2022. 3
- [73] Xizhou Zhu, Weijie Su, Lewei Lu, Bin Li, Xiaogang Wang, and Jifeng Dai. Deformable detr: Deformable transformers for end-to-end object detection. In *ICLR*, 2020. 2, 3, 6, 12
- [74] Maximilian Zipfl and J Marius Zöllner. Towards traffic scene description: The semantic scene graph. In *ITSC*, 2022. 3
- [75] Jannik Zürn, Johan Vertens, and Wolfram Burgard. Lane graph estimation for scene understanding in urban driving. *IEEE RA-L*, 2021. 2

Appendix

A. Implementation Details

A.1. Architecture

Backbone and View Transform. We adopt a ResNet-50 [23] with an FPN [39] to obtain multi-scale image features. Following previous works [73, 36], we use the output features from stage $S_{8\times}$, $S_{16\times}$ and $S_{32\times}$ of ResNet-50, where the subscripts $n \times$ indicates the downsampling factor. At the FPN, the features are transformed into a fourlevel output with an additional $S_{64\times}$ level. The number of output channels of each level is set to 256. Then we adopt a simplified view transformer with 3 encoder layers proposed in BEVFormer [36, 70]. Note that we do not utilize temporal information in this paper, and thus the temporal self-attention layer in the BEVFormer encoder degenerates to a deformable attention [73] layer. We transform the image features into four BEV grids with different heights of $\{-1.5m, -0.5m, +0.5m, +1.5m\}$ relative to the ground. The size of BEV grids is set to 200×100 .

Deformable Decoder Layers. We inherit most of the decoder layer design from Deformable DETR [73]. For the traffic element branch, we use 100 initial queries $q=[q_p,q_o]\in Q_t$, where q_p is utilized to generate the initial reference point, and q_o is the initial object query. The dimension of q is set to 256. Each decoder layer contains three operations: self-attention with 8 heads, deformable attention with 8 heads and 4 offset points, and a two-layer feedforward network with 512 channels in the middle layer. After each operation, a dropout layer with a ratio of 0.1 and a layer normalization is applied. For the centerline branch, all settings are kept the same as in the traffic element branch, except that the number of queries Q_l is set to 200.

Embedding Network. Following each decoder layer of the traffic element branch, an embedding network is employed. The embedding network is a two-layer MLP, in which the output channels are 512 and 256 respectively. In between the MLP, we include a ReLU activation function and a dropout layer.

Graph Convolutional Network. We utilize a simplified version of the Graph Convolutional Network (GCN) [32] as our GNN layer. Given an input matrix $Q^i \in \mathbb{R}^{N \times C}$, with N representing the number of nodes and C denoting the number of channels, the output of the operation is:

$$Q^{i'} = \sigma \Big(T^i Q^i \mathbf{W}^i \Big), \tag{9}$$

where $\mathbf{W}^i \in \mathbb{R}^{C \times C}$ is the learnable weight matrix, $T^i \in \mathbb{R}^{N' \times N}$ describes the adjacency matrix with N' output

nodes, and $\sigma(\cdot)$ is the activation function. The GCN acts as the network architecture for feature propagation, while detailed implementation could vary based on the topological construction in SGNN, *i.e.*, the naive scene graph structure (SG) and the elaborately designed knowledge graph (SKG).

Vanilla Scene Graph. After computing the matrices T_{ll} and T_{lt} of the graphs, a feature propagation process is executed using the GCN layer, where only the centerline queries are updated. Note that the matrices T_{ll} and T_{lt} are inferred without gradients during training.

Scene Knowledge Graph. We utilize a modified GCN layer, which is described in the paper, for feature propagation on the SKG. As in the vanilla scene graph, the matrices K_{ll} and K_{lt} are inferred without gradients during training. It is worth mentioning that the gradient is also not propagated through the classification score S_t of the traffic element during the calculation on SKG.

Prediction Heads. The prediction head for perception comprises a classification head and a regression head. For the traffic element branch, the classification head is a single-layer MLP, which outputs the sigmoid probability of each class. The regression head is a three-layer MLP with ReLU as the activation function in between, which predicts the normalized coordinates of 2D bounding boxes in the form of $\{cx, cy, width, height\}$. For centerline, the classification head consists of a three-layer MLP with LayerNorm and ReLU in between, which predicts the confidence score. The regression head is a three-layer MLP with ReLU, which predicts the normalized point set in the shape of 11×3 for a centerline.

Given the instance queries \widetilde{Q}_a and \widetilde{Q}_b with 256 feature channels, the topology head first applies a three-layer MLP:

$$\widetilde{Q}'_a = \mathrm{MLP_a}(\widetilde{Q}_a), \ \widetilde{Q}'_b = \mathrm{MLP_b}(\widetilde{Q}_b),$$
 (10)

where the number of output channels is 128. For each pair of queries $\tilde{q}'_a \in \widetilde{Q}'_a$ and $\tilde{q}'_b \in \widetilde{Q}'_b$, the output is the confidence of the relationship:

$$conf. = \mathrm{sigmoid}\Big(\mathrm{MLP_{top}}\big(\mathrm{concat}(\tilde{q}_a', \tilde{q}_b')\big)\Big), \quad (11)$$

where the MLP is independent in different types of relationships.

A.2. Training Details

Input. The resolution of input images is 2048×1550 , except for the front-view image which is in the size of 1550×2048 and is cropped into 1550×1550 . For data augmentation, resizing with a factor of 0.5 and color jitter is used by default.

Loss. The $\mathcal{L}_{det_{\text{TE}}}$ is decomposed into a classification, a regression, and an IoU loss:

$$\mathcal{L}_{det_{\text{TE}}} = \lambda_{cls} \cdot \mathcal{L}_{cls} + \lambda_{reg} \cdot \mathcal{L}_{reg} + \lambda_{iou} \cdot \mathcal{L}_{iou}, \quad (12)$$

where λ_{cls} , λ_{reg} , and λ_{iou} is set to 1.0, 2.5, and 1.0 respectively. The classification loss \mathcal{L}_{cls} is a Focal loss. Note that the regression loss \mathcal{L}_{reg} is an L1 Loss calculated on a normalized format of $\{cx, cy, width, height\}$, while the IoU loss \mathcal{L}_{iou} is a GIoU loss computed on the denormalized coordinates. For centerline detection, the $\mathcal{L}_{det_{LC}}$ comprises a classification and a regression loss:

$$\mathcal{L}_{det_{LC}} = \lambda_{cls} \cdot \mathcal{L}_{cls} + \lambda_{reg} \cdot \mathcal{L}_{reg}, \tag{13}$$

where λ_{cls} and λ_{reg} is set to 1.5 and 0.0075 respectively. Note that the regression loss is calculated on the denormalized 3D coordinates.

For topology reasoning, we adopt the same Focal loss but different weights on different types of relationships:

$$\mathcal{L}_{top} = \lambda_{top_{ll}} \cdot \mathcal{L}_{top_{ll}} + \lambda_{top_{lt}} \cdot \mathcal{L}_{top_{lt}}, \qquad (14)$$

where both $\lambda_{top_{ll}}$ and $\lambda_{top_{lt}}$ are set to 5.0.

B. Experiment Setup

B.1. Dataset

The OpenLane-V2 dataset [51] provides different types of annotations. Centerlines are described in the form of lists of points. Each list is ordered and comprises 201 points in 3D space. Statistically, about 90% of frames have more than 10 centerlines while about 10% have more than 40. Traffic elements follow the typical labeling style as in 2D detection. Each element is denoted as a 2D bounding box on the front view image, with its attribute. There are 13 types of attributes, including unknown, red, green, yellow, go_straight, turn_left, turn_right, no_left_turn, no_right_turn, u_turn, no_u_turn, slight_left, and slight_right. In the adjacency matrices, an entry (i, j) is positive (i.e., 1) if and only if the elements at i and j are connected. Statistically, most of the lanes have one predecessor and successor. The number of connections is up to 7, as a lane leads to many directions in a complex intersection. For the correspondence between centerlines and traffic elements, the majority have less than 5 correspondence while a tiny number of elements have up to 12. In summary, the dataset contains great topological complexity in the driving scenes, and raises huge challenges for algorithms to perceive and reason about the environment accurately.

B.2. Metrics

Perception. The DET score is the typical mean average precision (mAP) in object detection. The DET $_t$ uses IoU

as the similarity measure and is averaged over different attributes $\mathbb A$ of traffic elements:

$$DET_t = \frac{1}{|\mathbb{A}|} \sum_{a \in \mathbb{A}} AP_a. \tag{15}$$

For lanes, it adopts the discrete Fréchet distance [14] to measure the geometric similarity of two directed curves, which are described as ordered lists of points. Specifically, given a pair of curves, namely a ground truth $v_l = [p_0, ..., p_{n-1}]$ and a prediction $\hat{v}_l = [\hat{p}_0, ..., \hat{p}_{k-1}]$, a coupling L is a sequence of pairs between points in v and \hat{v} :

$$(p_{a_1}, \hat{p}_{b_1}), ..., (p_{a_m}, \hat{p}_{b_m}),$$
 (16)

where $0 = a_1 \le a_i \le a_j \le a_m = n-1$ and $0 = b_1 \le b_i \le b_j \le b_m = k-1$ for all i < j. Then the norm ||L|| of a coupling L is defined as the distance of the most dissimilar pair in L. The Fréchet distance of a pair of curves is the minimum norm of all possible coupling that:

$$D_{\text{fréchet}}(v_l, \hat{v}_l) = min\{||L|| \mid \forall \ possible \ L\}. \tag{17}$$

Based on the given similarity measure, the DET_l score is averaged over match thresholds of $\mathbb{T} = \{1.0, 2.0, 3.0\}$:

$$DET_l = \frac{1}{|\mathbb{T}|} \sum_{t \in \mathbb{T}} AP_t.$$
 (18)

Note that the defined BEV range is relatively large compared to other lane detection datasets, so accurate perception of lanes in the distance would be hard. Thresholds \mathbb{T} are relaxed based on the distance between the lane and the ego car.

Beseids, the Chamfer distance [15] for an additional metric $DET_{l.chamfer}$ ignores direction of lanes:

$$D_{\text{chamfer}}(v_{l}, \hat{v}_{l}) = \frac{1}{2} \left(\frac{1}{|v_{l}|} \sum_{p \in v_{l}} \min_{\hat{p} \in \hat{v}_{l}} ||p, \hat{p}||_{2} + \frac{1}{|\hat{v}_{l}|} \sum_{\hat{p} \in \hat{v}_{l}} \min_{p \in v_{l}} ||\hat{p}, p||_{2} \right).$$

$$(19)$$

The set of thresholds $\mathbb{T}_{chamfer}$ is set to $\{0.5, 1.0, 1.5\}$.

Reasoning. The TOP score is an mAP metric adapted from the graph domain. Specifically, given a ground truth graph G=(V,E) and a predicted one $\hat{G}=(\hat{V},\hat{E})$, it builds a projection on the vertices such that $V=\hat{V}'\subseteq\hat{V}$, where the Fréchet and IoU distances are utilized for similarity measure among lane centerlines and traffic elements respectively. Inside the predicted \hat{V}' , two vertices are regarded as connected if the confidence of the edge is greater than 0.5. Then the TOP score is the averaged vertice mAP between (V,E) and (\hat{V}',\hat{E}') over all vertices:

$$TOP = \frac{1}{|V|} \sum_{v \in V} \frac{\sum_{\hat{n}' \in \hat{N}'(v)} P(\hat{n}') \mathbb{1}(\hat{n}' \in N(v))}{|N(v)|}, \quad (20)$$

where N(v) denotes the ordered list of neighbors of vertex v ranked by confidence and P(v) is the precision of the i-th vertex v in the ordered list. The TOP_{ll} is for topology among centerlines on graph (V_l, E_{ll}) , and the TOP_{lt} for topology between lane centerlines and traffic elements on graph $(V_l \cup V_t, E_{lt})$.

Overall. The primary task of the dataset is scene structure perception and reasoning, which requires the model to recognize the dynamic drivable states of lanes in the surrounding environment. The OpenLane-V2 Score (OLS) summarizes metrics covering different aspects of the primary task:

$$OLS = \frac{1}{4} \left[DET_l + DET_t + f(TOP_{ll}) + f(TOP_{lt}) \right], (21)$$

where DET and TOP describe performance on perception and reasoning respectively, and f is the square root function. We omit the OLS metric in the main paper due to its high dependence on the traffic element detection results and argue that the overall evaluation metric is worthy of further exploration. We will provide more details and analysis in the section below (Appendix C.1).

B.3. Baseline Model

To perform ablations on the proposed SGNN, we compare it to a baseline network without feature propagation. In the baseline model, we set the parameters β_{ll} and β_{lt} to 0. As a result, the SGNN is degraded as an MLP, and the supervision of topology reasoning only occurs at the final decoder layer. The concatenation and down-sampling operations, as well as the traffic element embedding, are also removed.

In the "LL only" setting, we set the β_{lt} parameter to 0. Similar to the baseline, we remove the concatenation and down-sampling operations, as well as the traffic element embedding. For "LT only", we set the β_{ll} parameter to 0, while other modules remain intact. In the "w/o embedding" setting, we remove the traffic element embedding network and use Q_t as the input of SGNN directly.

B.4. Re-implementation of SOTA Methods

We adapt three state-of-the-art methods from centerline detection (STSU [5]) or map element detection (VectorMapNet [17] and MapTR [38]) into the OpenLane-V2 benchmark for a fair comparison.

STSU. The original model utilizes EfficientNet-B0 [60] as the backbone and detects centerlines and vehicles under the monocular setting. It employs a BEV positional embedding and a DETR head to predict three Bezier control points for each centerline, and uses object queries in the decoder to predict the connectivity of centerlines. To adapt to the

multi-view inputs, we re-implement STSU by replacing the original backbone with ResNet-50 and aligning the image input resolution with our model. Subsequently, we compute and concatenate the BEV embedding of images from different views. The concatenated embedding is then fed into the DETR encoder. We retain the original DETR decoder to predict the Bezier control points, which are interpolated into 11 equidistant points as outputs. The lane-lane relationship prediction head of STSU is preserved as well. For the newly added traffic element detection branch and lane-traffic element topology head, we adopt the same design as in TopoNet to ensure a fair comparison.

VectorMapNet utilizes a DETR-like decoder to estimate key points and an auto-regressive module to generate detailed graphical information for a laneline instance. It uses a smaller input image size with a shorter edge length of 256. We increase the length to 775 while maintaining the aspect ratio. The backbone setting is aligned with TopoNet. The perception range is defined as $\pm 30m \times \pm 15m$ in the original setting, but we expand it to $\pm 50m \times \pm 25m$. The centerline outputs of VectorMapNet are interpolated to fit our setting during the prediction process. For topology prediction, we use the key point object queries in the VectorMapNet decoder as instance queries of centerlines. We implement the modification on the given codebase of VectorMapNet while retaining other settings. However, due to their lack of support for 3D centerlines, we only predict 2D centerlines in the BEV space and ignore the height dimension.

MapTR. We align the original backbone setting with TopoNet. The perception region is expanded to $\pm 50m \times \pm 25m$. We adopt MapTR to predict 11 points for each centerline. For topology prediction, we use the average of point queries of an instance in the MapTR decoder as the object query of a centerline. The traffic element head and the topology head are with the same setting as in TopoNet. The implementation is also done on the open-source codebase of MapTR. Due to the lack of support for 3D centerlines, we only predict 2D centerlines in BEV and ignore the height dimension during inference, as in the re-implementation of VectorMapNet.

C. Experiments

C.1. Detailed Results

Due to the limited space, we omit part of the results in the main manuscript. We report evaluation results under all metrics in this section.

Comparison with State-of-the-art. In Table 4, we provide DET_t and OLS besides the metrics in the main paper. It is observed that though traffic element is better detected in

Data	Method	\mid DET $_l\uparrow$	$\mathrm{DET}_{l,\mathrm{chamfer}} \uparrow$	$TOP_{ll} \uparrow$	$\mathrm{DET}_t \uparrow$	$TOP_{lt} \!\!\uparrow$	OLS↑
	STSU [5]	12.0	11.5	0.3	62.3	10.1	27.9
	VectorMapNet [41]	11.3	13.4	0.1	58.5	6.2	24.5
All	MapTR [38]	8.3	<u>17.7</u>	0.2	60.7	5.8	24.3
7	MapTR* [38]	8.3	<u>17.7</u>	<u>1.1</u>	<u>60.7</u>	<u>10.1</u>	<u>30.2</u>
	TopoNet (Ours)	22.1	20.2	2.7	59.1	14.9	34.0
	STSU [5]	10.8	7.4	0.1	62.0	8.3	26.0
sgu	VectorMapNet [41]	<u>11.8</u>	11.4	0.0	59.5	5.5	23.7
ssii	MapTR [38]	7.0	<u>15.9</u>	0.1	<u>60.1</u>	4.5	23.0
Crossings	MapTR* [38]	7.0	<u>15.9</u>	0.8	<u>60.1</u>	8.2	<u>28.4</u>
0	TopoNet (Ours)	19.7	18.2	2.1	57.3	10.8	31.1
l uo	STSU [5]	9.2	10.0	0.4	58.6	7.1	25.3
lati	VectorMapNet [41]	8.1	6.3	0.1	<u>56.3</u>	5.1	22.5
Isolation	MapTR [38]	7.6	12.9	0.2	56.2	4.8	22.4
	MapTR* [38]	7.6	12.9	0.8	56.2	<u>8.1</u>	<u>26.7</u>
Geo.	TopoNet (Ours)	14.2	<u>12.6</u>	1.2	56.2	10.4	28.3

Table 4. Comparison with state-of-the-art methods under three data splits. DET_t and OLS are added to the table in the main paper. TopoNet outperforms all previous works by a wide margin, especially in directed centerline perception and topology reasoning despite having a lower traffic element detection score. *: OLS and topology reasoning evaluation based on matching results on Chamfer distance.

Type	Method	\mid DET $_l\uparrow$	$\mathrm{DET}_{l,\mathrm{chamfer}} \uparrow$	$TOP_{ll} \uparrow$	$\mathrm{DET}_t \uparrow$	$TOP_{lt} \uparrow$	OLS↑
-	Baseline	21.0	20.8	2.4	58.0	13.6	32.8
SG	+ LL only + LT only TopoNet-SG	20.9 21.0 21.7	19.8 19.6 20.2	2.4 2.6 2.4	60.8 60.3 61.6	13.0 15.2 15.5	33.3 34.1 34.5
SKG	+ LL only + LT only TopoNet-SKG	21.6 22.0 22.1	21.4 20.3 20.0	2.5 2.7 2.7	59.2 59.4 59.1	14.5 14.8 14.9	33.7 34.1 34.0

Table 5. Ablation on the design of scene graph neural network. DET_{l, chamfer} and OLS are added in the appendix table. Separating traffic elements and learning different graph weights based on their attributes (SKG) has a slight negative impact on traffic element detection, compared with SG. Due to the scale of results under different metrics, OLS is largely affected by the relatively high 2D detection results.

Method	\mid DET $_l\uparrow$	$\mathrm{DET}_{l,\mathrm{chamfer}} \uparrow$	$TOP_{ll} \uparrow$	$\mathrm{DET}_t \uparrow$	$TOP_{lt} \uparrow$	OLS↑
w/o embedding	19.1	18.2	2.6	59.8	14.9	33.4
TopoNet	22.1	20.2	2.7	59.1	14.9	34.0

Table 6. **Ablation on traffic element embedding.** OLS is included in the appendix. TE embedding effectively filters out irrelevant spatial information in the PV space and extracts high-level semantic knowledge to help centerline detection and lane topology reasoning.

Method	mIoU(%)↑
HDMapNet [35] TopoNet (Ours)	18.3 29.5

Table 7. Comparison with state-of-the-art BEV segmentation-based method. TopoNet remarkably outperforms the previous approach.

other algorithms, the proposed TopoNet outperforms them by a large margin in centerline perception and topology reasoning. Since all methods adopt the same traffic element head, we hypothesize the gap could result from the focus on lane topology optimization and separation of semantic knowledge, as shown in the SKG ablation.

Backbone	\mid DET $_l\uparrow$	$\mathrm{DET}_{l,\mathrm{chamfer}} \uparrow$	$TOP_{ll} \uparrow$	$\mathrm{DET}_t \!\!\uparrow$	$TOP_{lt} \!\!\uparrow$	OLS↑
ResNet-50	1	20.2	2.7		14.9	
Swin-tiny	22.5	21.7	2.6	71.7 (+12.6)	17.8	38.2

Table 8. **Results on Swin Transformer backbone.** With a superior backbone, TopoNet achieves significant improvement in 2D traffic element detection, leading to further progress on lane-traffic element relationship reasoning. Yet, the effect on lane topology is slight.

Ablations. In Table 5 and Table 6, the additional performance metrics namely DET_{l,chamfer} and OLS are provided. We can find that incorporating traffic element information advances DET_l performance while slightly hindering the $DET_{l,chamfer}$ score, indicating that traffic elements help to distinguish the direction of lanes and suppress some prediction results. Note that DET_{l,chamfer} is adopted to compare with previous map learning techniques, which is not the target in topology reasoning. Employing SKG to learn different graph weights based on their attributes may result in a slightly negative impact compared to using SG in the context of traffic element detection. As shown in Table 5, due to the scale of results under different metrics, OLS is largely affected by the relatively high 2D detection results. A higher OLS does not represent a superior topology reasoning ability of the algorithm, which we believe should be a much more essential factor in the task.

C.2. Additional Experiments

Comparison on BEV Segmentation. We provide a comparison to a state-of-the-art segmentation-based map learning approach, HDMapNet [35]. The prediction results of our method are rendered to BEV with a fixed line width of 0.75m, and the mIoU metric is adopted following common segmentation tasks. We reproduce HDMapNet on the OpenLane-V2 benchmark with an enlarged BEV perception range of $\pm 50m \times \pm 25m$ to get aligned with TopoNet. As shown in Table 7, TopoNet significantly surpasses HDMapNet by 11.2 points in terms of mIoU, verifying the advance of our framework.

Results on Swin Transformer Backbone. We present results of TopoNet with a Swin Transformer backbone [42] in Table 8. A stronger feature extractor enhances the 2D traffic element detection performance remarkably. It further results in the improvement on TOP_{lt} , while the effect on lane topology is slight.

D. Qualitative Results

We present visualizations of TopoNet with other state-of-the-art methods under different scenarios, including intersections in Fig. 5, missing-annotations in Fig. 6, and adversarial weather condition in Fig. 7. TopoNet demonstrates its superiority and robustness on perception and topology reasoning performance over previous works. Specifically,

it is observed that STSU generates a great amount of false positive centerline predictions, which also leads to its poor performance in topology reasoning as shown in Table 4. Meanwhile, MapTR is on-par with TopoNet on centerline perception when using Chamfer distance as the similarity measure, but it gets unsmooth results and a significant performance drop on the Fréchet distance.

E. Failure Case Analysis

Here we define failure cases as those severely deviating from the ground truth, and summarize their scenarios into two main categories: (1) large-area occlusion by vehicles, vegetation, and background buildings; (2) some long-tail scenarios such as parks and parking spots. Fig. 8 shows a case where a bus occludes the intersection in the front view image. TopoNet fails to predict lanes and the topology, especially those in the left half of the crossing. In a long-tail case as depicted in Fig. 9, the road topology is not regular as in straight highways or intersections, and all algorithms fail to provide correct road structure. A large-scale dataset and learning techniques such as active learning, are promising to solve these failure cases in a real-world deployment.

F. License of Assets

The training data are from the OpenLane-V2 dataset [51] and the Argoverse 2 Sensor dataset [66], which are under the CC-BY-NC-SA 4.0 license. The evaluation code in the OpenLane-V2 dataset is under the Apache-2.0 license. We integrate the pre-trained ResNet model and part of the BEV-Former [36] implementation in our code, which are under the MIT license and Apache-2.0 license respectively.

Two subfigures in Fig. 1 in the main paper are from the BEVFusion paper [43] and the VectorMapNet paper [41]. They use GPL-3.0 license and Apache-2.0 license respectively for public usage.

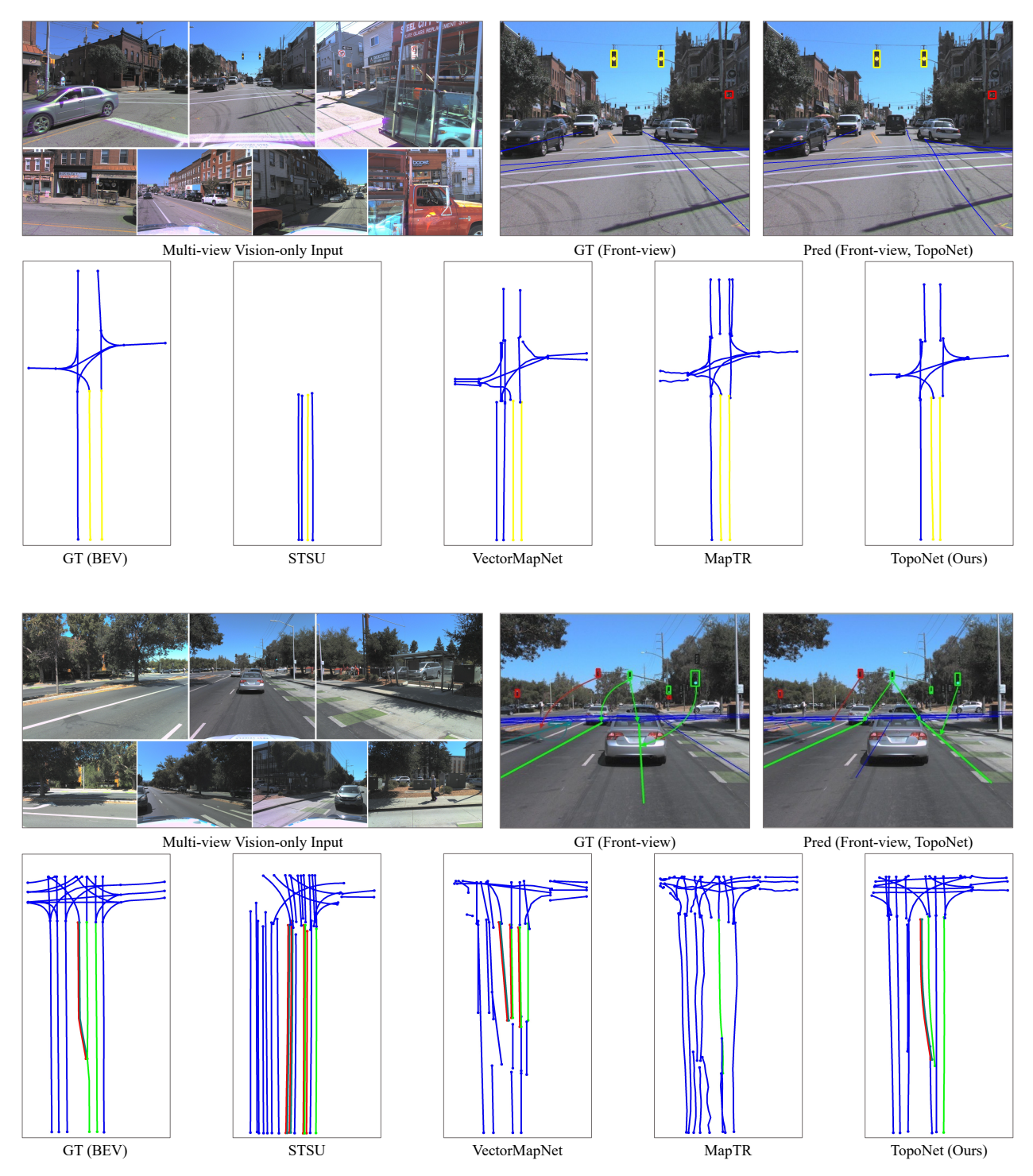


Figure 5. **Qualitative results** of TopoNet and other algorithms under two complex intersections. TopoNet outperforms other SOTA methods in lane graph prediction (BEV view), especially in terms of the centerlines inside the intersections. It also achieves superior performance than previous approaches to build connections between traffic elements and lanes (front-view, and correspondingly colored lines in BEV). Colors denote categories of traffic elements. The connectivity lines are not shown in the top case cause the corresponding centerlines exist in the back view.



Figure 6. **Visualization of an annotation missing case.** In this case, a relationship annotation between the traffic light and the centerline is missing, as there is no colored centerline in GT(BEV). TopoNet successfully predicts the connection (colored result in BEV; no connection line in front-view due to the centerline being in back-view).

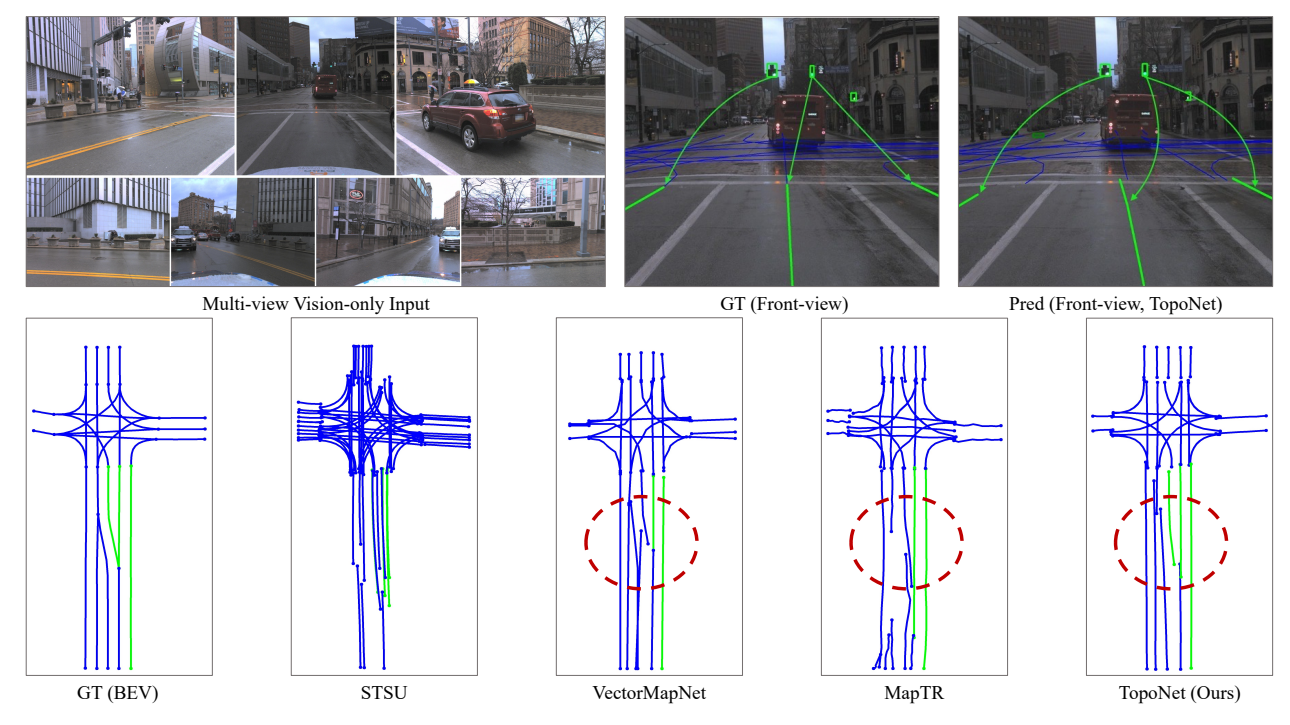


Figure 7. **Qualitative results under adversarial weather.** TopoNet generates more robust detection and topology reasoning results than other algorithms, such as the forking topology behind the vehicle (shown in the red circle).

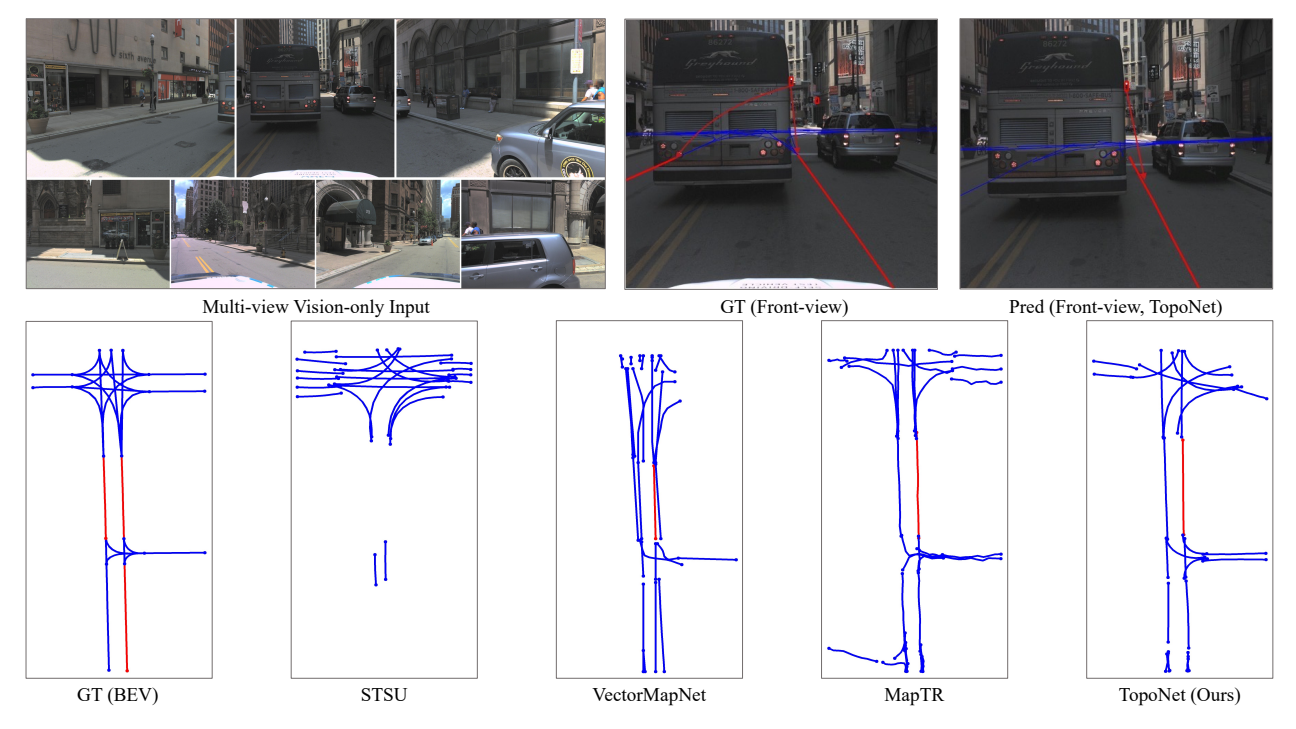


Figure 8. **Failure case under large-area occlusion.** TopoNet fails to predict centerlines and the lane graph in the intersection with a large bus colluding in front. Note that the relationship between the left lane and the red light is an incorrect annotation where our algorithm reasons about the direction of the left lane and avoids the false positive prediction.



Figure 9. **Failure case in a long-tail scenario.** The centerlines around the park construct an uncommon lane graph visualized in BEV. Though TopoNet generates partial correct results on the right, the overall performance of the topology reasoning is unsatisfactory.